PRAMANA
— journal of
physics

Vol. 64, No. 2
February 2005
pp. 229–238

Time-gated optical imaging through turbid media using stimulated Raman scattering: Studies on image contrast

K DIVAKAR RAO, H S PATEL, B JAIN and P K GUPTA
Biomedical Applications Section, Centre for Advanced Technology, Indore 452 013, India
E-mail: kdivakar@cat.ernet.in

MS received 23 July 2004; revised 3 November 2004; accepted 18 December 2004

Abstract. In this paper, we report the development of experimental set-up for time-gated optical imaging through turbid media using stimulated Raman scattering. Our studies on the contrast of time-gated images show that for a given optical thickness, the image contrast is better for sample with lower scattering coefficient and higher physical thickness, and that the contrast improves with decreasing value of anisotropy parameters of the scatterers. These results are consistent with time-resolved Monte Carlo simulations.

Keywords. Time-gated imaging; stimulated Raman scattering; image contrast.

PACS Nos 42.30.-d; 42.65.Dr; 87.63.Lk

1. Introduction

There exists considerable interest in the use of optical techniques for biomedical imaging. This is motivated by the potential of optical techniques to provide sub-millimeter resolution imaging without the need for ionizing radiation and associated risks [1,2]. The fundamental problem with optical imaging is that in contrast to X-rays, optical photons are strongly scattered in tissue, which leads to a blurring of the image. Several approaches can be used to pick out the useful image bearing light from the background multiply scattered light [3]. One approach exploits the fact that the multiply scattered photons take longer time to emerge from the scattering medium as compared to the ballistic or snake-like components, which essentially travel in the forward direction and thus arrive earlier. Therefore, by the use of appropriate time gating techniques, image-bearing photons can be filtered. Time gating can be achieved using fast electronic instrumentation such as gated optical image intensifiers [4], holography with femtosecond pulses [5], or by using intensity dependent non-linear optical gates such as the optical Kerr effect [6], dye-based optical amplifier [7] etc. Duncan *et al* [8] and Mahon *et al* [9] exploited time gating by stimulated Raman scattering (SRS) for selective amplification of image bearing part to demonstrate a direct two-dimensional imaging of objects through

turbid media with optical path length τ of $\sim$30 ($\tau = d \times \mu_s$ where μ_s is the scattering coefficient and d is the thickness of the sample). However, there is no detailed report on the effect of tissue optical properties like scattering coefficient, thickness of the sample, and scattering anisotropy factor g on the image contrast using this technique. This aspect has been addressed in the present manuscript. Our studies show that for a given optical thickness, contrast is better for sample with lower scattering coefficient (higher physical thickness) and the contrast improves with decreasing value of anisotropy parameter of the scatterers. These results are consistent with time-resolved Monte Carlo simulations.

2. Experimental details

A schematic of the set-up used for experiments is shown in figure 1. The second harmonic output of a picosecond Nd:YAG laser (continuum PY61C-10, 532 nm, 27 ps, up to 25 mJ, 10 Hz) was split into two beams in the power ratio of 40 : 60. The lower power beam ($\sim$2 mJ per pulse) was used to pump the 100 cm long Raman oscillator cell filled with H_2 at 30 atm in a near confocal geometry to generate 683 nm Stokes output. The high power beam was collimated and used to pump a 50 cm Raman amplifier also filled with H_2 at 30 atm. The vibrational dephasing time in H_2 at 30 atm is approximately 400 ps implying that the SRS process was in the transient regime. Typical conversion efficiencies of the Stokes generation in the oscillator were found to be $\sim$20%. The amplifier gain was estimated to be $\sim 10^4$–10^5. The oscillator was operated in saturation regime to minimize shot-to-shot fluctuation of the Stokes output. Typical amplitude fluctuation of first Stokes out-

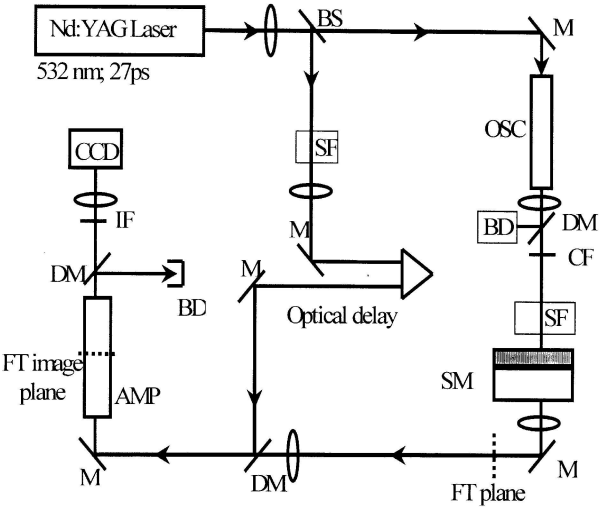

Figure 1. Schematic of the time-gated SRS set-up: BS – beam splitter; M – mirror; DM – dichroic mirror; CF – color filter; IF – interference filter, SF – spatial filter; SM – scattering medium; OSC – oscillator cell; AMP – amplifier cell; BD – beam dump. Dotted lines represent Fourier transform (FT) planes.

put at 683 nm was comparable to the fluctuations in the input pump beam (∼8% RMS). The Stokes output was separated from pump and the higher order Stokes and anti-Stokes output by using proper high- and low-pass filters. The spatially filtered and collimated Stokes beam was used to illuminate the object kept in a 10 mm cuvette containing a scattering medium prepared using various concentrations of Intralipid® solution or aqueous suspension of monodispersed polystyrene microspheres of different sizes. The transmitted scattered light from the sample was collected using a lens and its Fourier transform was relayed through the Raman amplifier. The amplified Stokes pulse was separated from the pump pulse using a dichroic mirror and interference filter. Inverse Fourier transform of the image was generated to obtain the image of object on a cooled scientific CCD camera (SBIG ST6).

The Stokes light emerging from the scattering medium gets temporally elongated due to multiple scattering. In order to preferentially amplify the image-bearing part of the transmitted light, the optical delay was adjusted so that the pump pulse temporally overlaps with the image bearing part of the transmitted pulse. This process was facilitated, by first optimizing the Raman amplification of the seed Stokes beam passing through the sample cuvette filled with water instead of the scattering sample. This ensured the temporal overlap between pump pulse and the image bearing part of the transmitted pulse in the presence of the scattering media. At this optimum delay, the image of the bar chart immersed in the scattering medium was seen on the CCD. However, no image was seen when the pump beam to the amplifier was blocked ensuring time-gated optical amplification.

3. Monte Carlo simulations

Time-resolved Monte Carlo simulations were carried out to record the temporal profile of the transmitted pulse through the scattering medium. For this, the steady-state Monte Carlo simulation code by Wang *et al* [10] was modified to incorporate a record of time history of each photon and thus generate the temporal profile of transmitted photons at the exit surface. Briefly, the photons launched in the medium (bounded by $Z = 0$ and $Z = d$, the thickness of the medium and assumed infinitely long in x and y directions) traverse exponentially distributed lengths s between successive scattering events. These random path lengths (s) were generated using the function $-\ln(\xi)/\mu_{\rm s}$, where ξ is a random number uniformly distributed between 0 to 1 and $\mu_{\rm s}$ is the scattering coefficient. The angle of scattering was sampled such that the angular distribution follows Henyey–Greenstein phase function [10]. The azimuthal angle was chosen from a uniformly distributed random number varying from 0 to 2π. After each scattering event the weight of photon was reduced by a factor of $(1 - \Delta W)$, ΔW being $\mu_a/(\mu_a + \mu_{\rm s})$. The simulation continues until the photons launched at the top surface of the slab are absorbed by the medium or emerge from one of the surface. Total path length traversed by the photon was estimated by summing all the individual path lengths. The time spent by the photon in the medium was obtained by dividing the length by velocity of light in the medium. The temporal profile of transmitted pulse was generated from the so determined temporal history of photons, which emerged from the bottom surface of

the medium. A total of 10^6 photons were launched to obtain temporal profile of the transmitted pulse. The results from the time-resolved code were verified to be in reasonable agreement with results predicted by approximate analytical expression based on time-dependent diffusion approximation [11].

4. Results and discussion

4.1 *Dependence of contrast on optimum delay*

In figure 2 we show the images of a bar chart (period ∼300 μm) kept inside a intralipid solution in a 10 mm cuvette with optical thickness τ of 15. The images were recorded at different optical delays of the pump. When the pump arrived 10 ps earlier than the optimum delay, the boundaries of the bar chart were sharp although the contrast was poor. At the optimum delay the contrast was better and the sharpness of the boundaries also increased. With a delay of 15 ps between the pump and Stokes only diffuse part of the Stokes beam was amplified as a result of which blurred image was seen. Since the maximum amplification in a transient

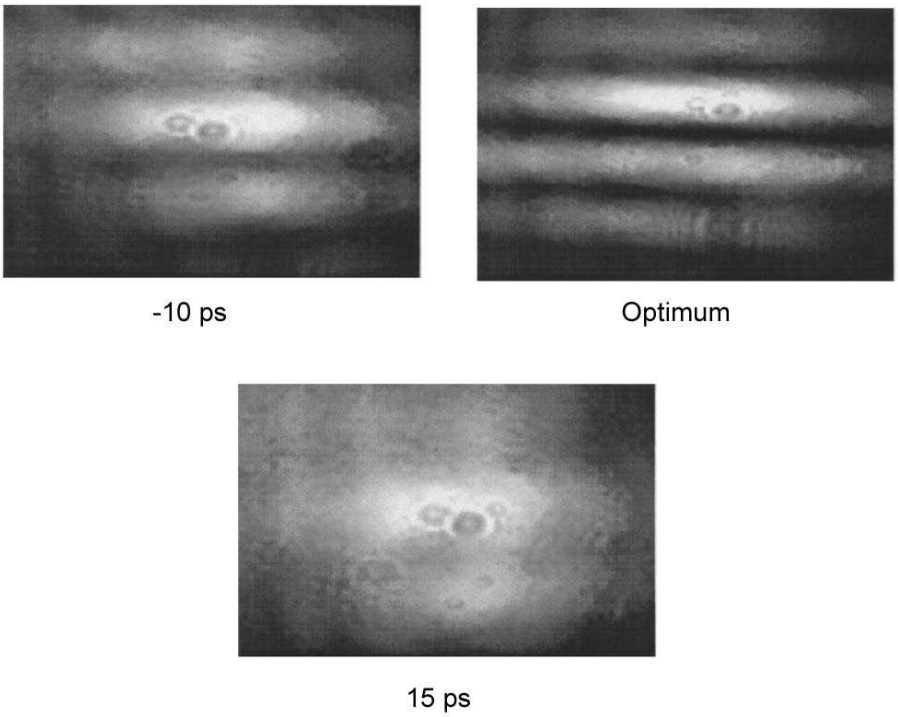

Figure 2. Time-gated, amplified images of a bar chart kept in a 10 mm thick cuvette containing intralipid solution ($\tau = 15$) in the path of seed Stokes beam. (**a**) Pump pulse precedes seed Stokes by 10 ps, (**b**) optimum delay of pump with respect to the seed Stokes, (**c**) pump pulse delayed by 15 ps compared to the optimum Stokes timing.

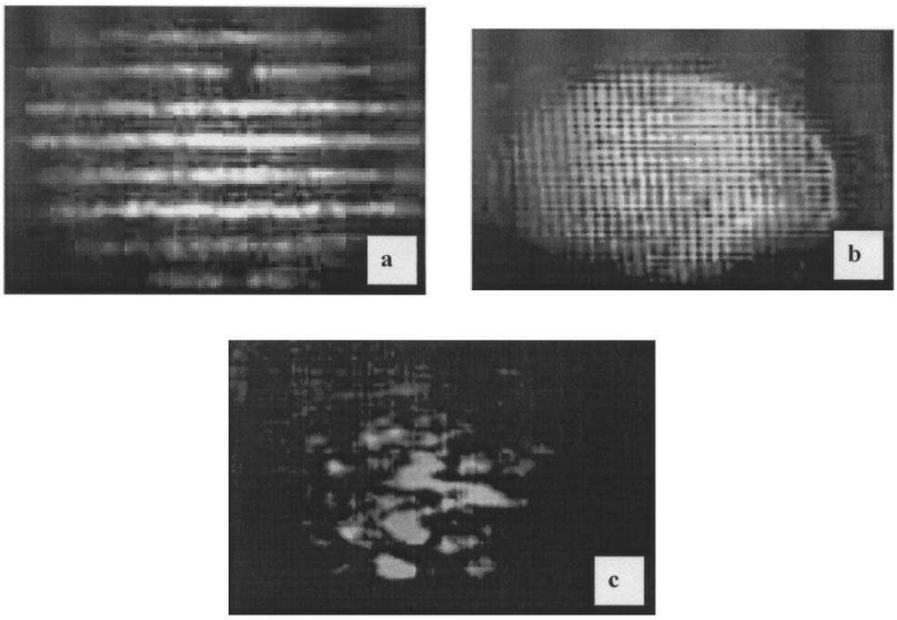

Figure 3. Time-gated, amplified images of objects placed inside a 10 mm thick cuvette containing intralipid solution having $\mu_s \sim 2.5$ mm^{-1} in the path of seed Stokes beam: (**a**) Single-shot image of resolution bar chart with a period 300 μm, (**b**) single shot image of square metallic grid with 30 μm metallic obstruction and 55 μm clear space, (**c**) background image when pump laser is blocked. Camera integration time in this case is 5 s.

Raman amplifier occurs when the seed Stokes beam precedes the pump pulse [12], the best image contrast does not occur at the zero delay between the pump and seed Stokes pulses. Further, the image contrast does not decrease symmetrically about the optimum delay position because at higher delays amplification of snake and diffuse photons degrades the image quality. In figures 3a and 3b we show the amplified time-gated image of a bar chart with period ∼300 μm (150 μm bar and 150 μm spacing) and a square metallic grid with 85 μm period (30 μm metal obstruction and 55 μm clear region) through intralipid solution with $\tau \sim 25$. Figure 3c shows typical background acquired when there is no amplification. The line-pair resolution achieved was ∼85 μm, which is in good agreement with the estimated spatial resolution of ∼61 μm of the set-up, based on the cut-off spatial frequency of the amplifier. It should however be noted that for a time-gated imaging set-up like this one, the limiting resolution is also dependent on scattering coefficient of the tissue and the optimum time-gate position as shown by Papaioannou *et al* [13].

4.2 *Dependence of contrast on anisotropy parameter*

To investigate the dependence of image contrast on the anisotropy parameter of the sample we imaged a bar chart (period 300 μm) through scattering samples

having the same optical thickness τ but different scattering anisotropy parameters (g). From the acquired images, contrast (C) was determined using the relation $C = (I_{\max} - I_{\min})/I_{\max}$, where $I_{\max}$ is the maximum intensity and $I_{\min}$ is the minimum intensity. Figure 4a shows the variation of contrast on the anisotropy parameter for a sample with optical thickness $\tau = 15$ and $\mu_s = 1.5$ mm^{-1}. In figure 4b we show the result of Monte Carlo simulations of the transmitted profiles for samples with different anisotropy parameters but fixed τ. It can be seen from the figure that there is considerable difference in the broadening as well as the diffuse transmitted intensity for samples with different g values. It is important to note that for samples having smaller g value, the multiply scattered photons are spread over a larger cone angle and time. Therefore, for a given collection angle, the contribution of late arriving diffuse photons will be less compared to the sample with high anisotropy parameter. Another important factor that would contribute to the observed better contrast with decreasing anisotropy parameter is the fact that the Raman amplifier's gain is higher for Stokes photons, which have the same polarization as the incident pump beam [14,15]. Since the polarization is preserved for the multiply scattered forward moving photons in anisotropic scatterers compared to the isotropic scattering, the image degradation is more for sample prepared using scatterers having higher g values leading to a poorer contrast.

4.3 *Dependence of contrast on physical thickness of the sample*

In figure 5 we show the image of a bar chart with a period of 300 μm recorded through two samples (polystyrene microspheres with mean diameter 1.08 μm) having the same optical thickness ($\tau = 15$) and g value but different physical thickness 10 mm (figure 5a) and 5 mm (figure 5b). The corresponding intensity variations in the image are displayed in figure 5c. The solid line in figure 5c is for 10 mm thickness sample whereas the dotted line is for 5 mm thick sample. Figure 6 shows the corresponding results of time-resolved Monte Carlo simulations of the transmitted profiles from the two samples with different physical thickness ($d = 10$ mm

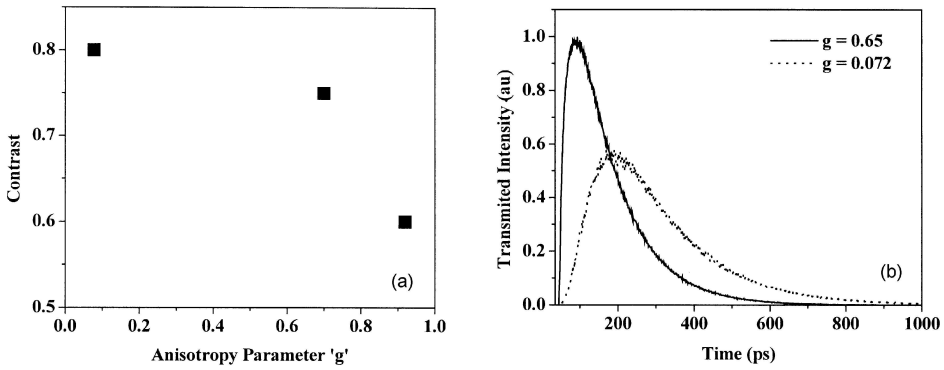

Figure 4. (**a**) Dependence of image contrast on anisotropy parameter for scattering coefficient $\mu_s = 1.5$ mm^{-1}, (**b**) Monte Carlo simulation of the transmitted profiles for same τ but different anisotropy values. Solid line is for $g = 0.65$ and dotted line for $g = 0.072$.

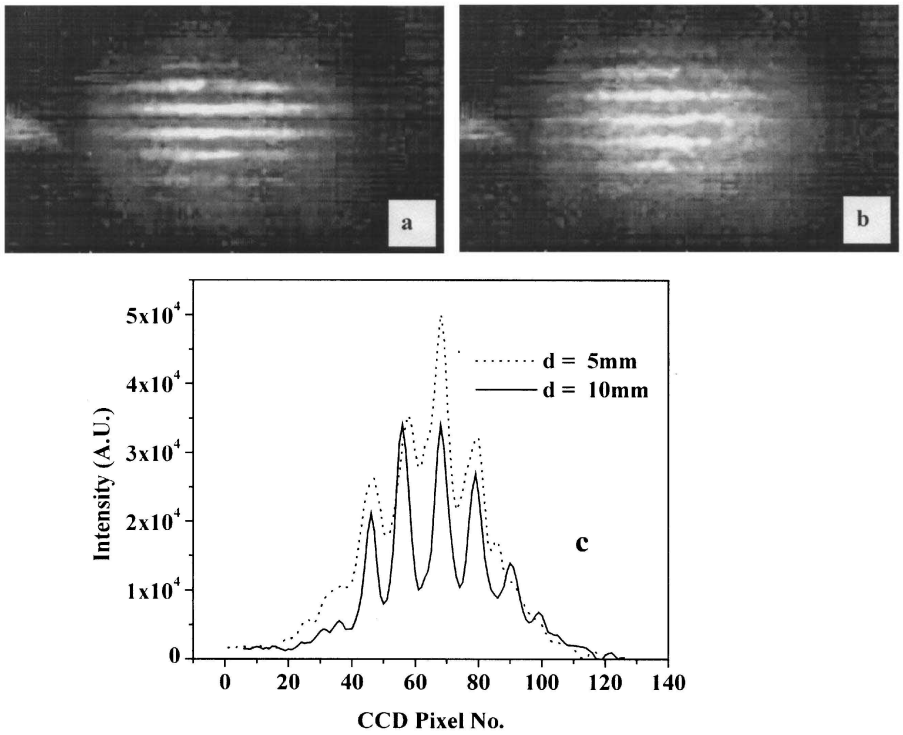

Figure 5. Time-gated, amplified images of bar chart (300 μm period) placed inside the scattering medium (polystyrene microspheres with mean diameter 1.08 μm and $\tau = 15$) with thickness of the scattering medium $d = 10$ mm (**a**) and $d = 5$ mm (**b**). The graph (**c**) shows the variation of intensity as a function of CCD pixel position. The solid line is for the thicker sample ($d = 10$ mm) and dotted line is for 5 mm sample.

and 5 mm) for $\tau = 15$. It can be seen from the figure that for the thick sample temporal profile of the transmitted pulse is broader with lower transmitted intensity compared with the thin sample. This observation is in agreement with the results of Wang *et al* [16] which showed that the samples having identical τ but different physical thickness results in different amount of broadening of an ultra-fast pulse propagating through such medium, broadening being more in sample having smaller scattering coefficient and correspondingly larger physical thickness. Thus for a fixed gate width, as is the case with time gating by the SRS amplification, discrimination of the diffuse photons is better for thicker samples compared to that for thinner samples (figure 5).

4.4 *Monte Carlo simulation and estimation of image contrast*

An estimate for the contrast can be obtained by estimating the contribution of quasi-ballistic photons to the image. Following Das *et al* [17], the intensity $I_{\mathrm{qb}}(\Delta t)$

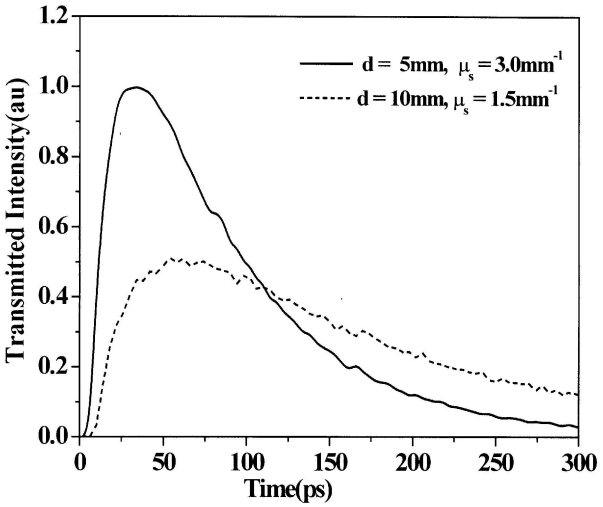

Figure 6. Time-resolved Monte Carlo simulation of the transmitted profile for two samples having same optical thickness but different scattering coefficients. Solid line is with $d = 5$ mm, $\mu_s = 3.0$ mm^{-1} and dotted line is with $d = 10$ mm, $\mu_s = 1.5$ mm^{-1}.

of quasi-ballistic components in a time gate of interval Δt from transit time t_{tr} to $t_{tr} + \Delta t$ through a slab of scattering sample was computed as

$$I_{qb}(\Delta t) = \alpha \int_{t_{tr}}^{t_{tr}+\Delta t} I(t)\mathrm{d}t,$$

where transit time $t_{tr} = nd/c$ is the time taken by straight moving ballistic photons to emerge from a sample with thickness d and refractive index n, c is the speed of light in vacuum. The collection factor α takes into account the fact that in a given imaging geometry, only a fraction of transmitted light is able to reach the detector. In our experimental set-up only $\sim 4\times10^{-4}$ of the transmitted snake light passes through the spatial filters to reach the amplifier cell. The transmitted intensity profile $I(t)$ is modeled using Monte Carlo simulation. Contribution of quasi-ballistic components to the image was calculated with incremental steps of 5 ps up to a maximum gate width of $\sqrt{3}t_{tr}$. The choice of $\sqrt{3}t_{tr}$ as the maximum gate width was motivated by results of Fishkin *et al* [18] where it was shown that the diffuse photons travel with a phase velocity of $c/n\sqrt{3}$.

To estimate the contrast of the image formed by ballistic and quasi-ballistic photons we assume a linear degradation of contrast from a value of 1 to 0 in the time interval of t_{tr} to $t_{tr} + \sqrt{3}t_{tr}$, i.e. the contrast of the image formed purely by ballistic photons is unity and that by diffuse photon is zero (no image). Contrast at different gate widths was estimated using weighted average of contrast due to ballistic and quasi-ballistic components with intensity of each component being taken as weight. In figure 7, we show the anisotropy parameter dependence of the contrast thus estimated for samples with scattering coefficient $\mu_s = 1.5$ mm^{-1}, $d = 10$ mm and for different gate widths. The anisotropy dependence of the contrast at a fixed

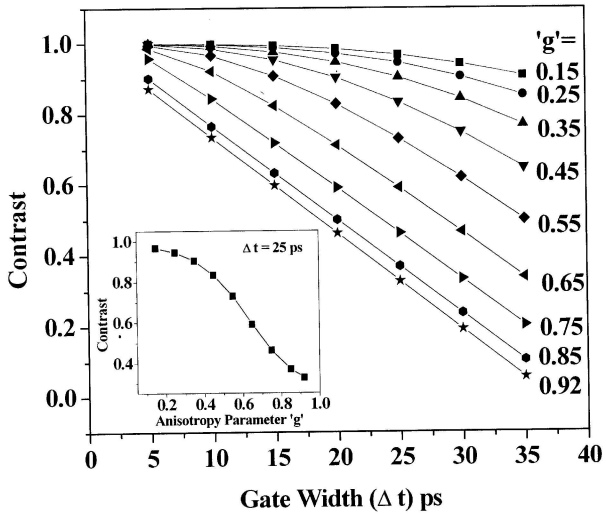

Figure 7. Time-resolved Monte Carlo simulation of the variation of contrast as a function of gate width for different anisotropy parameters. Inset shows the variation of contrast with anisotropy parameter at a fixed gate width of 25 ps.

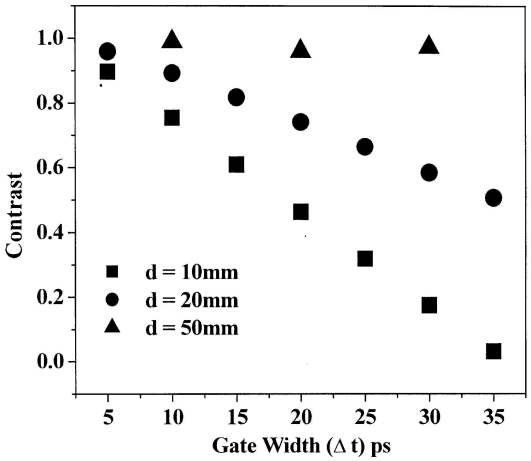

Figure 8. Time-resolved Monte Carlo simulation of variation of contrast as a function of gate width at different physical thickness keeping $\tau = 15$.

gate width of 25 ps is shown in the inset. It can be seen from the figure that for all gate widths, best contrast is observed for a sample having smaller g value. Figure 8 shows the results of the Monte Carlo simulations for thickness dependence of the contrast for samples having identical optical thickness and anisotropy values. Results show improvement in contrast with increasing physical thickness. This is because of the fact that with increase in physical thickness and hence the transit time $t_{\rm tr}$, the arrival time of diffuse component ($\sqrt{3}t_{\rm tr}$) is well-separated from the

image bearing components (see figure 6) leading to better contrast. Both the results are in good qualitative agreement with the experimental observations. It is to be noted that the simple empirical modeling of the image contrast leads to a good qualitative agreement with the experimental data.

5. Conclusions

We have demonstrated the use of time gating by SRS to image objects through a 10 mm cuvette containing intralipid solution ($\mu_s \sim 2.5$ mm^{-1}) with a spatial resolution up to $\sim$85 μm. Our studies on dependence of contrast on anisotropy parameter g and thickness of the sample show that for a given τ, contrast is better for sample having lower μ_s and further, the contrast increases with decreasing value of g. The experimental observations were validated by time-resolved Monte Carlo simulation.

Acknowledgements

The authors thank Ajay Kak of glass blowing facility (CAT Indore) for the technical help and Sendhil Raja for useful conversations.

References

[1] J C Hebden, S R Arridge and D T Delpy, *Phys. Med. Biol.* **42**, 825 (1997)
[2] H Ramachandran, *Curr. Sci.* **76**, 1334 (1999)
[3] C Dunsby and P M W French, *J. Phys.* **D36**, R207 (2003)
[4] M E Zevallous, S K Gayen, B B Das, M Alrubaiee and R R Alfano, *IEEE J. Select. Top. Quant. Elect.* **5**, 916 (1999)
[5] H Chen, Y Chen, D Dlworth, E Leith, J Lopez and J Valdmanis, *Opt. Lett.* **16**, 487 (1991)
[6] L Wang, P P Ho, C Liu, G Zhang and R R Alfano, *Science* **253**, 769 (1991)
[7] S Marengo, C Pepin, T Goulet and D Houde, *IEEE J. Select. Top. Quant. Electr.* **5**, 895 (1999)
[8] M D Duncan, R Mahon, L L Tankersley and J Reintjes, *Opt. Lett.* **16**, 1868 (1991)
[9] R Mahon, M D Duncan, L L Tankersley and J Reintjes, *Appl. Opt.* **32**, 7425 (1993)
[10] L H Wang, S L Jacques and L Q Zheng, *Comput. Methods Prog. Biomed.* **47**, 131 (1995)
[11] M Patterson, B Chance and B C Wilson, *Appl. Opt.* **28**, 2331 (1989)
[12] M D Duncan, R Mahon, L L Tankersley and J Reintjes, *J. Opt. Soc. Am.* **B9**, 2107 (1992)
[13] D G Papaioannou, G W 't Hooft, J J M Baselmans and M J C van Gemert, *Appl. Opt.* **34**, 6144 (1995)
[14] L M Bel'dyugin and E M Zemskov, *Sov. J. Quantum Electron.* **7**, 628 (1977)
[15] C Go, J Lee and J S Chang, *Appl. Opt.* **34**, 2671 (1995)
[16] Q Z Wang, X Liang, L Wang, P P Ho and R R Alfano, *Opt. Lett.* **20**, 1498 (1995)
[17] B B Das, F Lieu and R R Alfano, *Rep. Prog. Phys.* **60**, 227 (1997)
[18] J Fishkin, S Fantini, M J van de Ven and E Gratton, *Phys. Rev.* **E53**, 2307 (1996)